Available online at www.sciencedirect.com
ScienceDirect
Chemical Physics 347 (2008) 288–299
Chemical Physics
www.elsevier.com/locate/chemphys

Further aspects of the roaming mechanism in formaldehyde dissociation

S.A. Lahankar [a], V. Goncharov [a], F. Suits [b], J.D. Farnum [c], J.M. Bowman [c], Arthur G. Suits [a,*]

[a] Department of Chemistry, Wayne State University, Detroit, MI 48202, United States
[b] Computational Biology Center, IBM T. J. Watson Research Center, Yorktown Heights, NY 10598, United States
[c] Department of Chemistry and Cherry L Emerson Center for Scientific Computation, Emory University, Atlanta, GA 30322, United States

Received 26 September 2007; accepted 6 November 2007
Available online 22 November 2007

Abstract

Recently we reported a novel "roaming" dissociation pathway of formaldehyde in which one of the H atoms strays far from the minimum energy reaction path, explores a broad region of the potential energy surface, then abstracts the remaining H atom to form molecular products, without going near the configuration of the conventional transition state saddle point. The detailed dynamics of the abstraction mechanism and its energy dependence have already been reported. Here, with a combination of experimental and theoretical results, we examine the roaming behavior at the energetic extremes. We show evidence of roaming below the threshold of the radical dissociation channel and consider the implications of this and the possible existence of a transition state for the roaming mechanism. We also show the occurrence of roaming up to $\sim$3200 cm^{-1} above the threshold of the triplet dissociation channel. In addition, we present results affording deeper insight into the dynamics of the roaming mechanism: we show evidence of roaming leading to CO in $v = 1$, and examine the issue of nuclear spin conservation during dissociation via the roaming mechanism.

Keywords: Photodissociation; Reaction dynamics; Excited states; Roaming atoms; Photochemistry

1. Introduction

Formaldehyde has been a prototype molecule in the study of spectroscopy and reaction mechanisms for decades [1–16]. It was the first polyatomic molecule on which a detailed spectroscopic investigation was carried out [1,2]. The relevant energy levels are given in Fig. 1. Its dissociation processes following excitation in the near ultraviolet, which take place after internal conversion to the ground state or intersystem crossing to the triplet, can be summarized as the following reactions [16]:

$$H_2CO(S_0) \rightarrow H_2 + CO \text{ (Channel 1)}$$
$$H_2CO(S_0) \rightarrow H + HCO \text{ (Channel 2)}$$
$$H_2CO(S_0) \rightarrow [H \cdots HCO] \rightarrow H_2 + CO \text{ (Channel 3)}$$
$$H_2CO(T_1) \rightarrow H + HCO \text{ (Channel 4)}$$
$$H_2CO(T_1) \rightarrow H + H + CO \text{ (Channel 5)}$$
$$H_2CO(S_1) \rightarrow H + H + CO \text{ (Channel 6)}$$

In the 1980s and early 1990s, the Moore group at Berkeley investigated the dissociation of formaldehyde via the molecular transition state (TS) to form CO and H_2 (channel 1) in detail [8,10,17–26]. The dissociation of formaldehyde via channel 1 yields rotationally hot CO ($j_{CO} = 21$–70) and vibrationally "cold" H_2($v_{H2} = 0$–5) [13,27]. The observation of rotationally hot CO was assigned [20] to impulsive dissociation via the TS, which has a skewed planar geometry with both H atoms on the same side of the CO [28–32]. The barrier for this dissociation is 27,720 cm^{-1} [10]. Recently Chambreau et al. reported a state-correlated investigation of the dissociation of formaldehyde via channel 1 [27]. A strong correlation between the rotational states of CO and the vibrational states of H_2 was observed up to $\sim$4100 cm^{-1} above the barrier for channel 1. This strong

* Corresponding author. Tel.: +1 631 632 1702; fax: +1 631 632 7960.
E-mail address: asuits@chem.wayne.edu (A.G. Suits).

0301-0104/$ - see front matter © 2007 Elsevier B.V. All rights reserved.
doi:10.1016/j.chemphys.2007.11.007

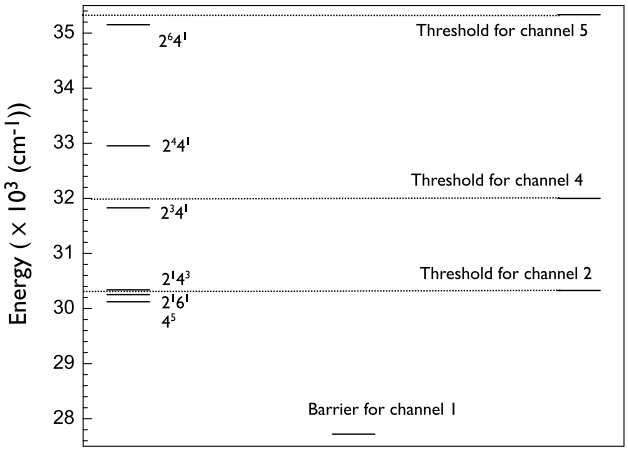

Fig. 1. Formaldehyde dissociation thresholds along with energy levels accessed in this investigation.

correlation is mainly dynamical in origin, a consequence of the highly repulsive exit channel and the skewed geometry of the TS [27]. It was also found that the correlation between the rotational states of H_2 and CO was very weak as noted earlier by Moore and coworkers.

Moore's group also investigated the conservation of nuclear spin in formaldehyde during the molecular dissociation via the $2^1 4^1$ transition [18]. Formaldehyde is a planar molecule with C_{2v} point group. Two nuclear spin modifications are possible for formaldehyde: *ortho*-formaldehyde and *para*-formaldehyde. *ortho*-Formaldehyde has odd K_a values and *para*-formaldehyde has even K_a values. Moore et al. reported that nuclear spin is conserved between formaldehyde and H_2 during the dissociation. That is, the dissociation of *ortho*-formaldehyde leads to formation of *ortho*-H_2 and the dissociation of *para*-formaldehyde leads to formation of *para*-H_2.

Formaldehyde also undergoes simple bond fission to form radical products H and HCO (Channel 2). This reaction is barrierless on the ground singlet surface. Kable and co-workers [11,33–37] and Wittig and co-workers [12] have studied the dynamics of this process. The threshold for channel 2 is 30327.6 cm^{-1} [37]. Dissociation via channel 2 yields high N HCO. The product HCO distribution from channel 2 is statistical and successfully modeled by phase space theory (PST). Radical dissociation of formaldehyde on the triplet surface (Channel 4) has a threshold of ~32 000 cm^{-1}, implying an exit barrier of ~1700 cm^{-1} [33]. However there is possible tunneling through the barrier of channel 4 following excitation to the $2^2 4^3$ transition at 31,555 cm^{-1} [34]. Dissociation of formaldehyde via channel 4 leads to low N HCO [33]. In this case, the product state distribution (PSD) is not statistical and cannot be described by PST. It was modeled as an impulsive dissociation similar to the approach used by Moore and co-workers for dissociation via channel 1. Recently Kable and Bowman and their co-workers have investigated the dynamics of dissociation of formaldehyde via channel 2 and channel 4 in detail [33,34].

In 2004, our group, in collaboration with the Bowman group at Emory, identified a new dissociation pathway of formaldehyde and termed it the roaming mechanism [13]. This reaction, anticipated in earlier studies [10], from the Moore group, starts as channel 2, although it lacks sufficient energy in the reaction coordinate to dissociate. One of the H atoms (to be denoted as H_R) roams around the HCO until it abstracts the remaining H (H_L) atom from HCO to form vibrationally hot H_2 ($v_{H2} = 5$–8) and rotationally cold CO ($j_{CO} = 0$–32) [13,14,38]. The dynamics of this H-abstraction have been examined in detail. The resulting high vibrational excitation in H_2 is due to the exoergic reaction occurring at long H–H distances. The H_L tends to leave HCO along its equilibrium bond angle irrespective of the position of H_R relative to the HCO. This leads to significant rotational excitation in product H_2 from roaming [14]. The roaming mechanism is a large amplitude motion that occurs in the H–HCO region of configuration space, with of course a minimum flux dividing surface and therefore a (variational) transition state. Thus, $H_2 + CO$ can be formed from two quite different pathways through two transition states; these two pathways are denoted as channels 1 (conventional) and channel 3 (roaming).

The roaming mechanism (channel 3) occurs on the singlet ground state and competes with channel 1 and channel 2. This was examined in detail experimentally and theoretically for excitation via the $2^1 4^3$ transition [14]. The overall branching between channel 3 and channel 1 was found to be 0.18:0.82. This was then used to estimate the energy dependence of the branching between channels 1 and 3 obtained from excitation spectra [15]. We found that as the available energy increases, channel 3 grows significantly relative to channel 1 [15]. These estimated branching fractions were combined with the theoretical estimates of branching of molecular products relative to radical products to yield overall multichannel branching. The branching results showed that as the available energy is increased from 30,300 to 32,000 cm^{-1}, the contribution of channel 1 drops from 0.8 to 0.15, the contribution of channel 2 increases from 0.0 to 0.75, and the contribution from channel 3 decreases from 0.18 to 0.10 [15].

In the present paper, we bracket the threshold for channel 3, thus determine the effective energy width of the roaming event and the energy of a possible saddle point "region" for the roaming pathway recently suggested by Harding and coworkers [39]. This is considered in light of quasiclassical trajectory (QCT) calculations on the fitted surface. We also report evidence of roaming leading to vibrationally excited product CO, explore roaming at very high excitation energies, and examine the issue of nuclear spin conservation during roaming dissociation.

2. Experiment

Formaldehyde for the experiment was prepared in situ with scheme used by Kable and co-workers [37], with modification to suit our experimental setup. A cylindrical tube

with several layers of paraformaldehyde and magnesium sulfate separated by glass wool was connected to a piezoelectric pulsed valve assembly and the entire system was heated to 60 °C using electrical heating tapes. The formaldehyde was seeded in two atm Ar and supersonically expanded into the source region. The beam was skimmed before entering the main chamber. Typical rotational temperatures under these conditions are ~10 K.

Formaldehyde photolysis was carried in the range 30,000–35,400 cm^{-1}. The dissociation laser beam was produced by doubling the output of a tunable dye laser pumped by the second harmonic of a nanosecond neodymium: yttrium aluminum garnet (Nd:YAG) laser. The photolysis energy was ~1.5–2.0 mJ/pulse. The product CO was probed using (2+1) resonance enhanced multiphoton ionization (REMPI) via the B-state around 230 nm. The probe laser beam was generated by sum frequency mixing of the third harmonic of an injection-seeded Nd:YAG laser with the fundamental of a dye laser (~654 nm) pumped by the second harmonic of the same Nd:YAG laser. The probe energy used was ~2.5–3.0 mJ/pulse.

Photolysis of formaldehyde followed by ionization of CO occurs between the repeller and first lens in the ion optics assembly. The ionized CO is then accelerated out of the interaction region and detected using our high-resolution DC slice imaging technique with a detector gate width of 60 ns. Details of this setup have been reported previously [40]. Detected ions were imaged by a charge-coupled device (CCD) camera and images were acquired and integrated with our IMACQ Megapixel imaging software [41]. The raw images were analyzed to yield product velocity distributions. Explicit treatment of finite slicing was also applied to account for the difference in slice width for slow versus fast photofragments [42]. The PHOFEX scans were acquired using a photomultiplier tube viewing the detector in conjunction with a digital oscilloscope, with the MCP gate expanded to 320 ns so that the full CO^+ ion signal was acquired. During scans, the laser wavelength was continuously monitored using a wavemeter. The photolysis and probe laser power was stable during all the PHOFEX scans and no power correction was required.

3. Theory

Investigations of the roaming region used the previously reported potential energy surface (PES) for formaldehyde [43]. The surface combines 15,668 CCSD(T) symmetry-unique energies with about 46,000 MR-CI symmetry-unique energies all calculated with the aug-cc-pVTZ basis set. The energies are fit with a set of Morse variables to obtain an analytic approximation to the PES of the system.

Quasi-classical trajectories have been simulated and reported on this system and are used in the detailed investigation of the present work [13,38,44]. The trajectories started at an initial geometry where one of the CH bonds has been stretched to about twice the equilibrium length. Zero-point energy was then randomized among the real normal modes and the excess energy was put into the imaginary normal mode in the form of kinetic energy. Approximate quantum states are assigned to the products of each trajectory using histogram binning of the classical quantities.

4. Results

Fig. 2 shows a high resolution PHOFEX scan of formaldehyde when the probe laser was set at j_{CO} 45, 15, and 10. We showed previously that when CO is probed at j_{CO} 45, only dissociation via channel 1 is observed, whereas when CO is probed at j_{CO} 15 or 10, only dissociation via channel 3 is observed [15]. Hence, PHOFEX at j_{CO} 45 is used as a proxy for dissociation via channel 1 and PHOFEX at j_{CO} 15, 10 are used as proxies for dissociation via channel 3. PHOFEX at j_{CO} 45 shows three vibrational bands of S_1 in this region: 4^5, 2^16^1, 2^14^3. However, PHOFEX scans at j_{CO} 15 and 10 show only the two higher energy vibrational bands of S_1, 2^16^1 and 2^14^3; the 4^5 band is missing. This implies that the threshold for the roaming pathway is between the 4^5 band (30,123 cm^{-1}) and the 2^16^1 transition (30,241 cm^{-1}). The vertical dotted line shows the experimental threshold of channel 2.

To further verify the PHOFEX scans, images were acquired after excitation of formaldehyde to $^rR_1(1)$ branch of 4^5 and $^pP_1(1)$ branch of 2^16^1 bands, with CO probed at j_{CO} 45 and 14. Fig. 3 shows these images and the corresponding translational energy distributions. In Fig. 3a and b, the vibrational distribution peaks at $v = 2$. This internal energy distribution of H_2 is similar to the internal distribution obtained previously via the 2^14^3 transition probed at j_{CO} 45, and it clearly represents dissociation via channel 1. In Fig. 3c the internal energy distribution of H_2 peaks at $v = 7$, $j_{H2} = 7$ and $v = 6$, $j_{H2} = 9$. This is

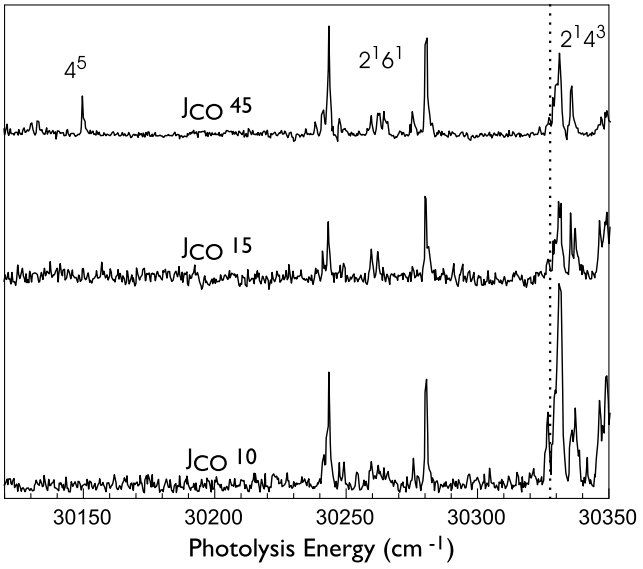

Fig. 2. PHOFEX spectra obtained with CO probe was set at indicated rotational level.

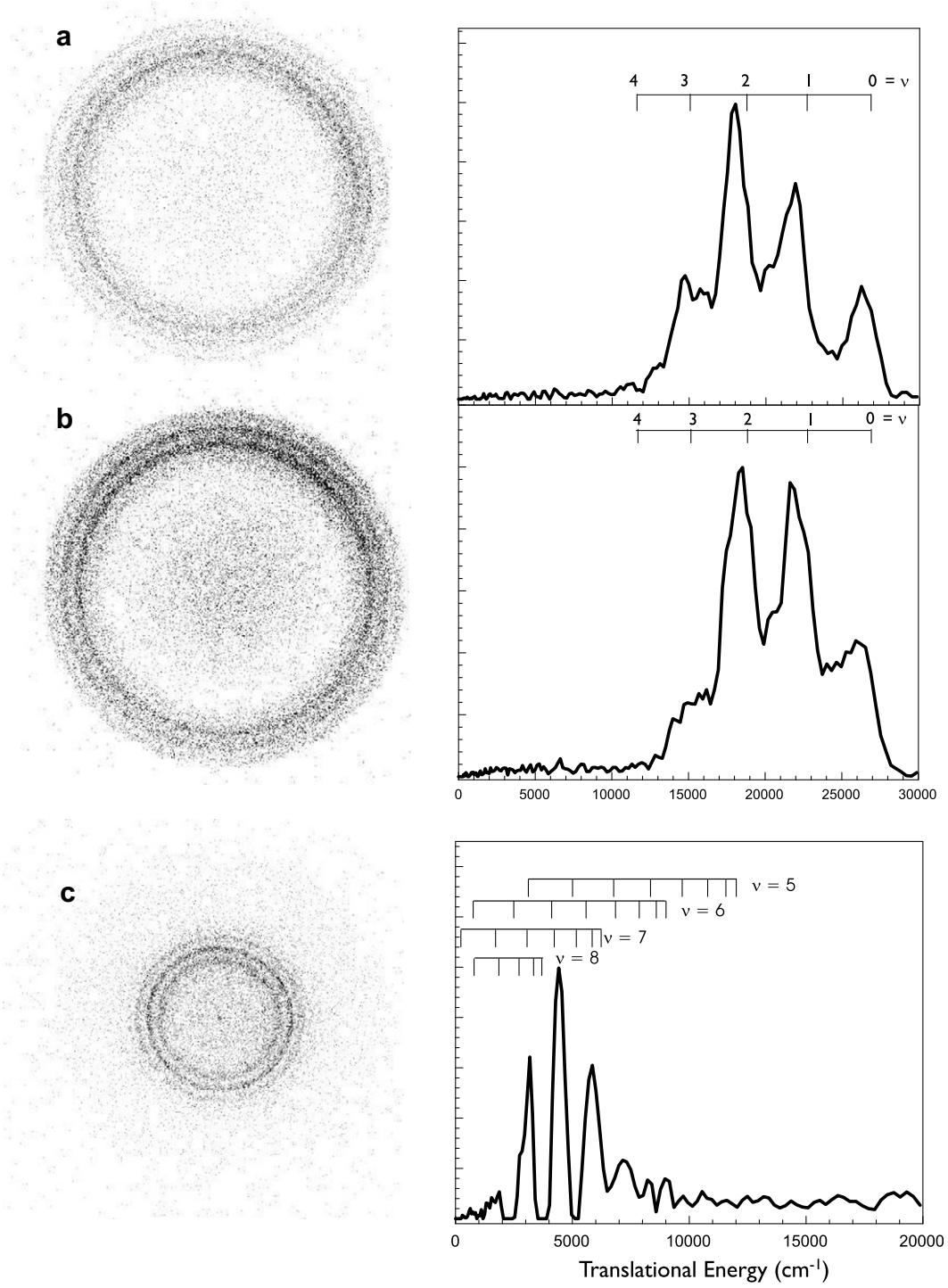

Fig. 3. Images (left) and translational energy distributions (right) acquired at: (a) 4^5 j_{CO} 45; (b) $2^1 6^1$ j_{CO} 45; (c) $2^1 6^1$ j_{CO} 14.

similar to the internal energy distribution obtained for low j_{CO} via the $2^1 4^3$ band, and can be explained by the roaming model. No signal was observed for the 4^5 band when CO is probed at j_{CO} 15 or 10.

A number of images and associated translational energy distributions obtained for low rotational levels of CO ($v = 0$) following photolysis at 35,217 cm^{-1} via the $2^6 4^1$ and $2^4 4^1$ bands are shown in Fig. 4. Fig. 4a and b show that the internal energy distribution of H_2 peaks at $v = 8$, 9 and goes up to $v = 10$, $j_{H2} = 7$. For the $2^4 4^1$ level (Fig. 4c) the internal energy distribution peaks at $H_2 v = 7$, 8 and goes up to $v = 9$, $j_{H2} = 7$.

Images and the corresponding translational energy distributions for low rotational levels of CO ($v = 1$) acquired after excitation of formaldehyde via the $2^4 4^1$ and $2^1 4^3$ bands are shown in Fig. 5. The internal energy distribution of H_2 peaks at $v = 7$, 8, $j_{H2} = 7$ for the $2^4 4^1$ band whereas it peaks at $v = 7$, $j_{H2} = 3$ and $v = 6$, $j_{H2} = 7$ for $2^1 4^3$ band.

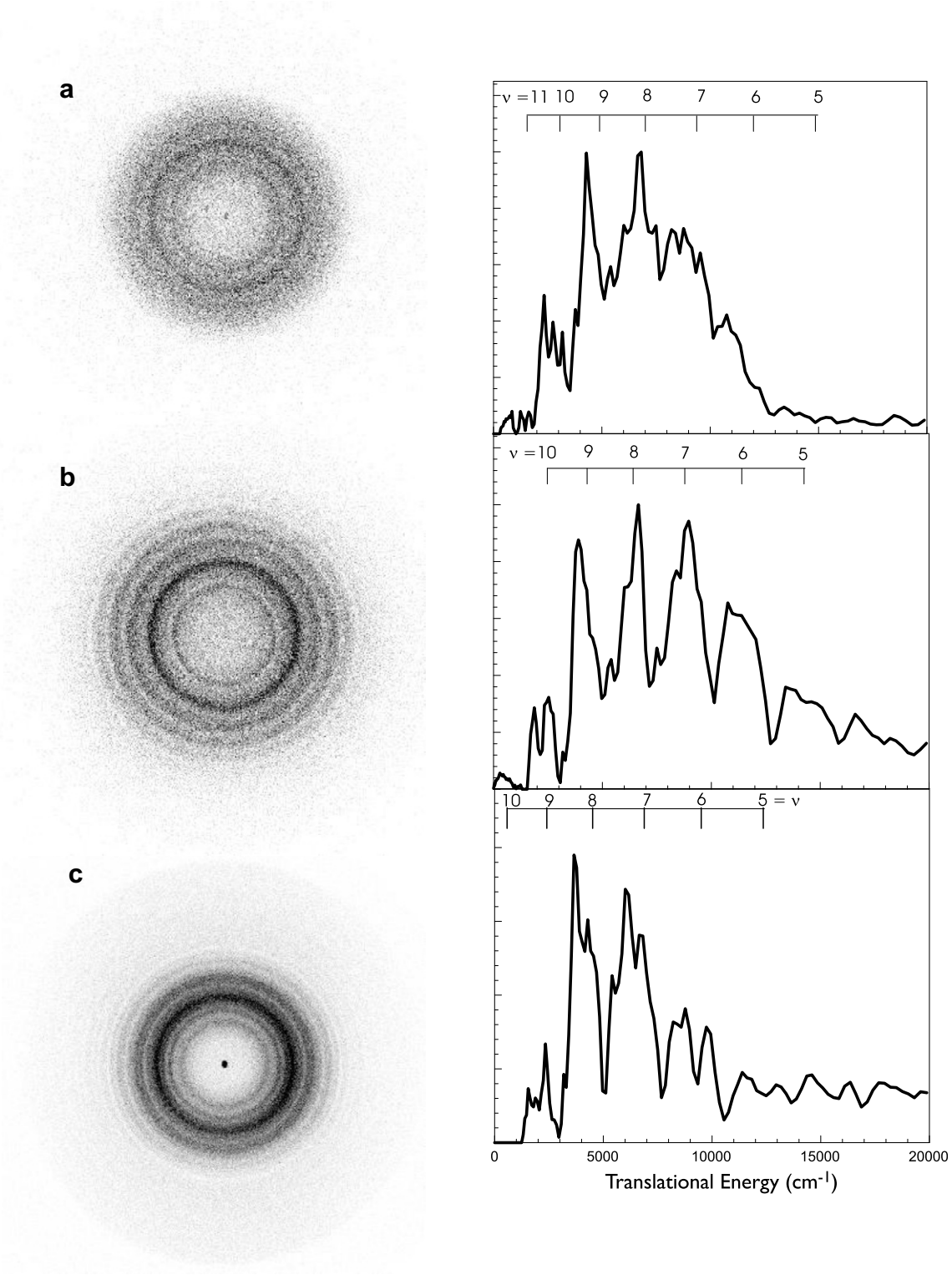

Fig. 4. Images (left) and translational energy distributions (right) acquired at: (a) 35,217 cm^{-1} j_{CO} 12; (b) $2^6 4^1$ j_{CO} 18; (c) $2^4 4^1$ j_{CO} 15.

The images and associated translational energy distributions in Fig. 6 were acquired by excitation of formaldehyde to the $2^2 4^1$ level and individually selecting (a) *ortho* and (b) *para*-formaldehyde. The *ortho*-formaldehyde is selected by excitation to the $^rR_1(1)$ branch of $2^2 4^1$ and *para*-formaldehyde is selected by excitation to $^rR_0(0)$ branch of the $2^2 4^1$ band. In the translational energy distributions, the dark curve is the result of *para*-formaldehyde dissociation whereas the light curve is from *ortho*-formaldehyde dissociation. The combs show the rovibrational assignment for dissociation to $j_{H2} = 6$, 8 for *para* H_2 and $j_{H2} = 7,9$ for *ortho* H_2.

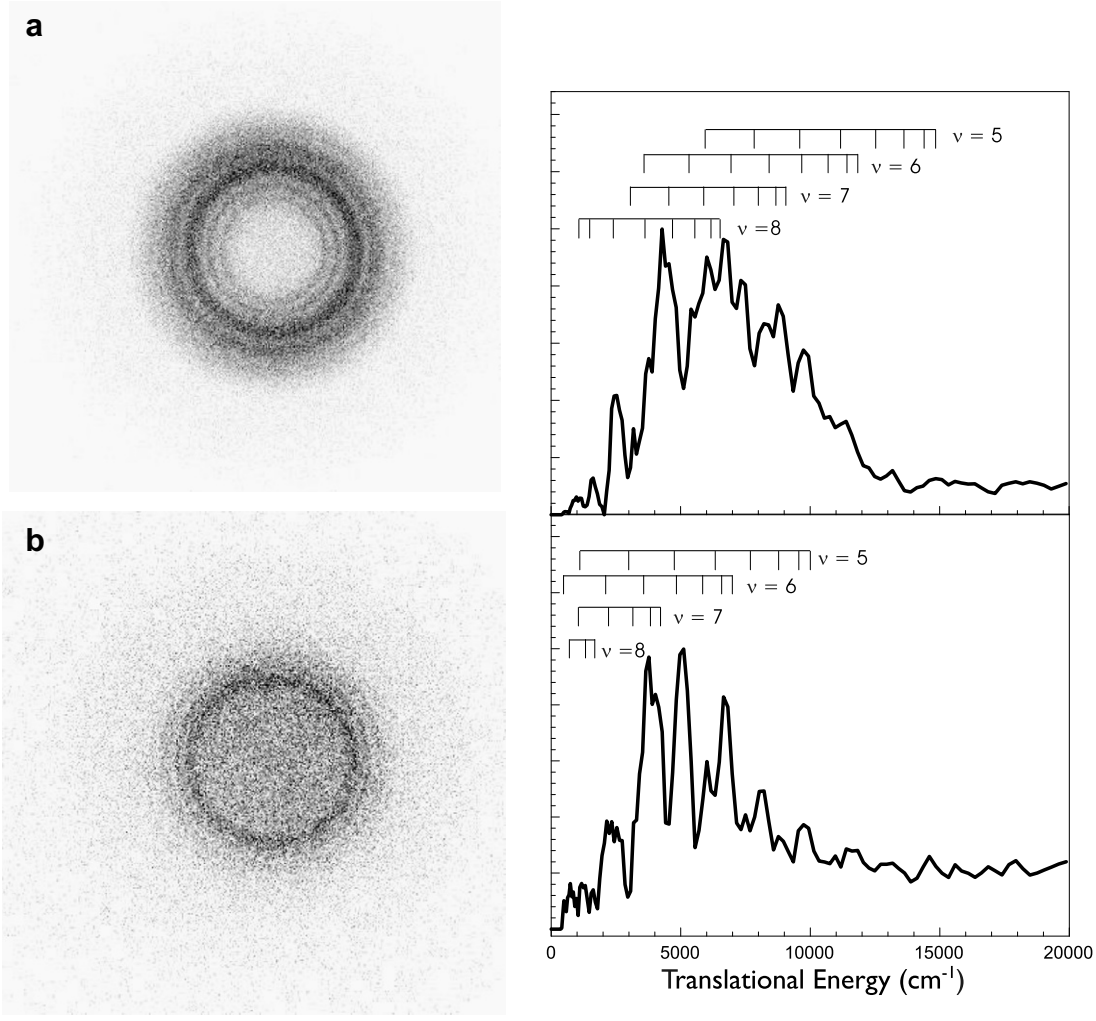

Fig. 5. Images (left) and translational energy distributions (right) acquired at: (a) $2^4 4^1 v = 1$, j_{CO} 14; (b) $2^1 4^3$ $v = 1$, j_{CO} 15.

5. Discussion

These new results probe several distinct aspects of the roaming mechanism in formaldehyde dissociation. In previous work we have shown this pathway to be the result of frustrated dissociation via the radical channel that leads to intramolecular H abstraction and distinct product state distributions in both CO and H_2. This was seen in the bimodal correlated product state distributions from experiment and illustrated dramatically in the dynamical calculations from the Bowman group. It was further confirmed in the match between theory and experiment in the energy dependence of the branching between channel 1 and channel 3. We now examine the implications of the new results presented in the preceding section.

5.1. Roaming threshold

We can consider the roaming process in two steps: first, the roaming excursion, and second, the abstraction reaction. The H_2 rovibrational distributions allowed us to examine aspects of the H abstraction dynamics leading to high H_2 vibrational excitation [14], and we showed that the abstraction reaction favors transfer of the HCO H atom along the HCO equilibrium direction regardless of the approach of the roaming atom. Furthermore, we found no strong constraint for roaming in the HCO plane. The PHOFEX spectra (Fig. 2) and associated images and translational energy distributions (Fig. 3) obtained below the radical threshold now allow us a detailed look at the initial phase of the roaming process leading up to the abstraction.

The PHOFEX spectra at j_{CO} 45 in Fig. 2 illustrate the expected presence of channel 1 following excitation to 4^5, $2^1 6^1$, and $2^1 4^3$ bands in S_1, an energy roughly 2500 cm^{-1} above the molecular transition state saddle point. However, the analogous spectra recorded at j_{CO} 10 and 15 suggest dissociation via channel 3 (roaming) at $2^1 6^1$, and $2^1 4^3$ but not 4^5. The images and associated correlated state distributions (Fig. 3c) clearly confirm that these low j_{CO} products are indeed the result of roaming. This is quite significant: these results allow us to bracket the occurrence of roaming in a window extending to roughly 100 cm^{-1} below the radical threshold. These results are particularly noteworthy in light of a recent report [39] from Harding

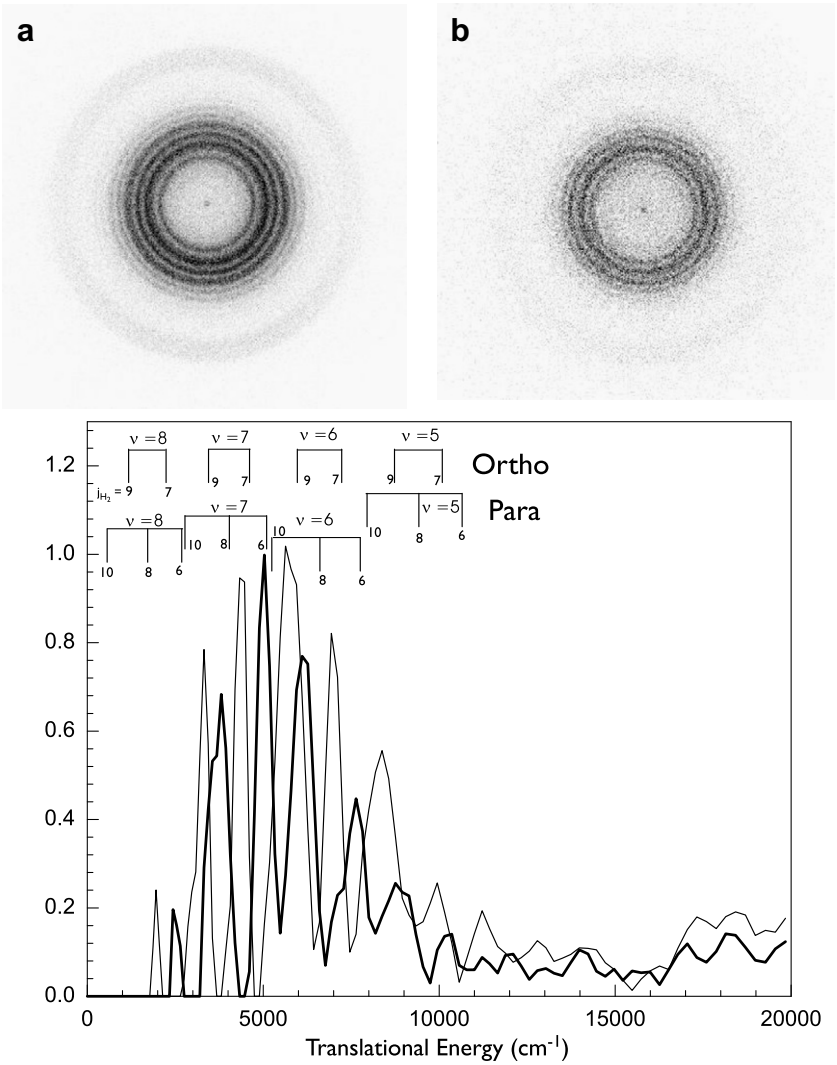

Fig. 6. Images (top) and translational energy distributions (bottom) acquired after excitation of: (a) *para* (dark line); (b) *ortho* (light line) transitions in $2^2 4^1$ and probed at j_{CO} 15.

et al., identifying a second (or possibly multiple) saddle point on the potential energy surface using CASPT2 and CAS+1+2+QC calculations. It is predicted to lie only 40–80 cm^{-1} below the radical threshold, with a C–H_R distance of 6.6 bohr and a nearly perpendicular position of the roaming atom with respect to the HCO plane. They report an imaginary frequency of 156 cm^{-1} and extremely low real frequencies of 22 and 83 cm^{-1} [39,45]. They note that the large amplitude, anharmonic nature of this roaming transition state (TS_R) suggests it should really be considered a "region" of the surface controlling the roaming reaction, not a well-defined TS. Motivated by Harding's result and our PHOFEX spectra, we have examined the fitted potential in the region reported for TS_R. Relevant scans of the PES are shown in Fig. 7 for several C–H_R distances as a function of in-plane (θ) and out-of-plane (φ) angles of H_R with respect to HCO in its equilibrium geometry. These scans show evidence for this barrier as a ridge surrounding the abstraction region in the center of the figures. For the scan at a C–H_R distance of 6.5 bohr the barrier on the PES is roughly 30 cm^{-1} below the PES D_e and at an out-of-plane angle of roughly 120° which is fully consistent with the TS_R result of Harding et al. Futhermore, the contours shown are spaced 30 cm^{-1} apart, underlining how flat this "saddle point" is. Our PHOFEX spectra also clearly support the notion of a barrier for the roaming reaction, although they necessarily place it >87 cm^{-1} below the radical dissociation asymptote, which is slightly below the lower limit suggested by Harding et al.

Our goal now is to understand the nature of the roaming excursion, its relation to TS_R, and the implications of this for the energy dependence of the roaming pathway. In our initial report, we included animations of two of the calculated trajectories: one characteristic of the roaming pathway and another representing a typical molecular dissociation via channel 1. We subsequently showed that the roaming pathway could be effectively visualized using a multidimensional plot of the entire trajectory showing only the two H atoms. In Fig. 8, we show similar trajectory "images" to shed light on these issues. These show one

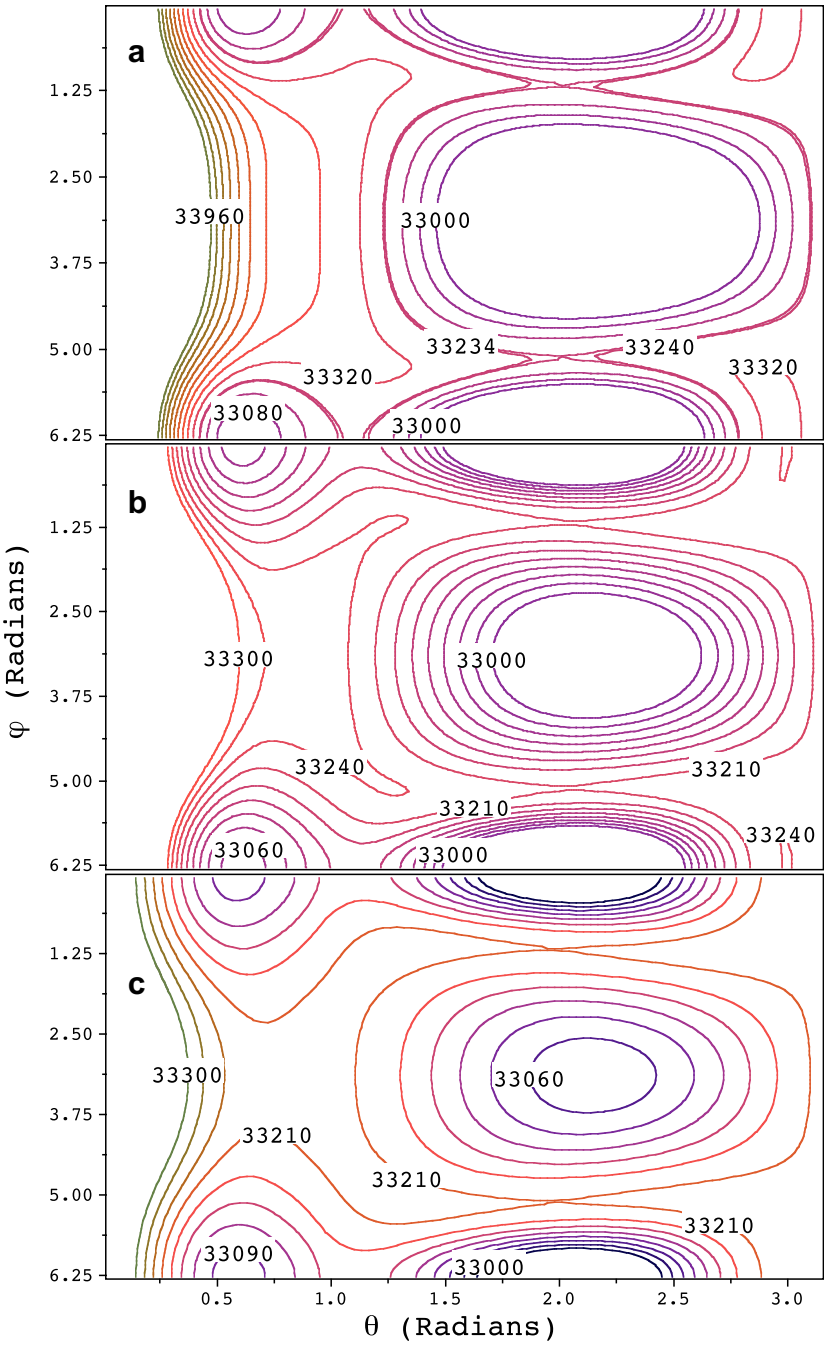

Fig. 7. Contours of the roaming hydrogen at fixed R_{CH} distance rotating around HCO in the radical equilibrium geometry. Panel (a) shows an energy range of 33,000–34,000 cm^{-1} with contour lines every 80 cm^{-1} for $R_{CH} = 6.0$ bohr. An extra contour line is added at 33,234 cm^{-1} to show the approximate threshold to hydrogen abstraction at this distance. Panels (b) ($R_{CH} = 6.614$ bohr) and (c) ($R_{CH} = 7.0$ bohr) show an energy range of 33,000–33,300 cm^{-1} with contour lines at every 30 cm^{-1}. The threshold at these distances is approximately 33,210 cm^{-1}.

non-roaming event (Fig. 8a), numerous examples of roaming trajectories (Fig. 8b–e), and finally, one roaming trajectory that yields vibrationally excited CO (Fig. 8f). Accompanying each trajectory image is a plot of the two C–H distances and total potential energy at each time step of the trajectory. The trajectories in Fig. 8a and b were performed at 36,200 cm^{-1} above the H_2CO global minimum while the remainder were run at 36,500 cm^{-1}, well above the saddle point identified by Harding and coworkers. (Note the harmonic zero-point energy from the PES is 5844 cm^{-1} and this energy must be subtracted from the total energies relative to the global minimum to make a direct correspondence with the experimental energies.)

These images and associated plots are rich in information. In the images, one can readily identify the pre-roaming accumulation of energy in the $C–H_R$ coordinate. During roaming, the potential energy oscillates about an average high value due mainly to HCO vibration and

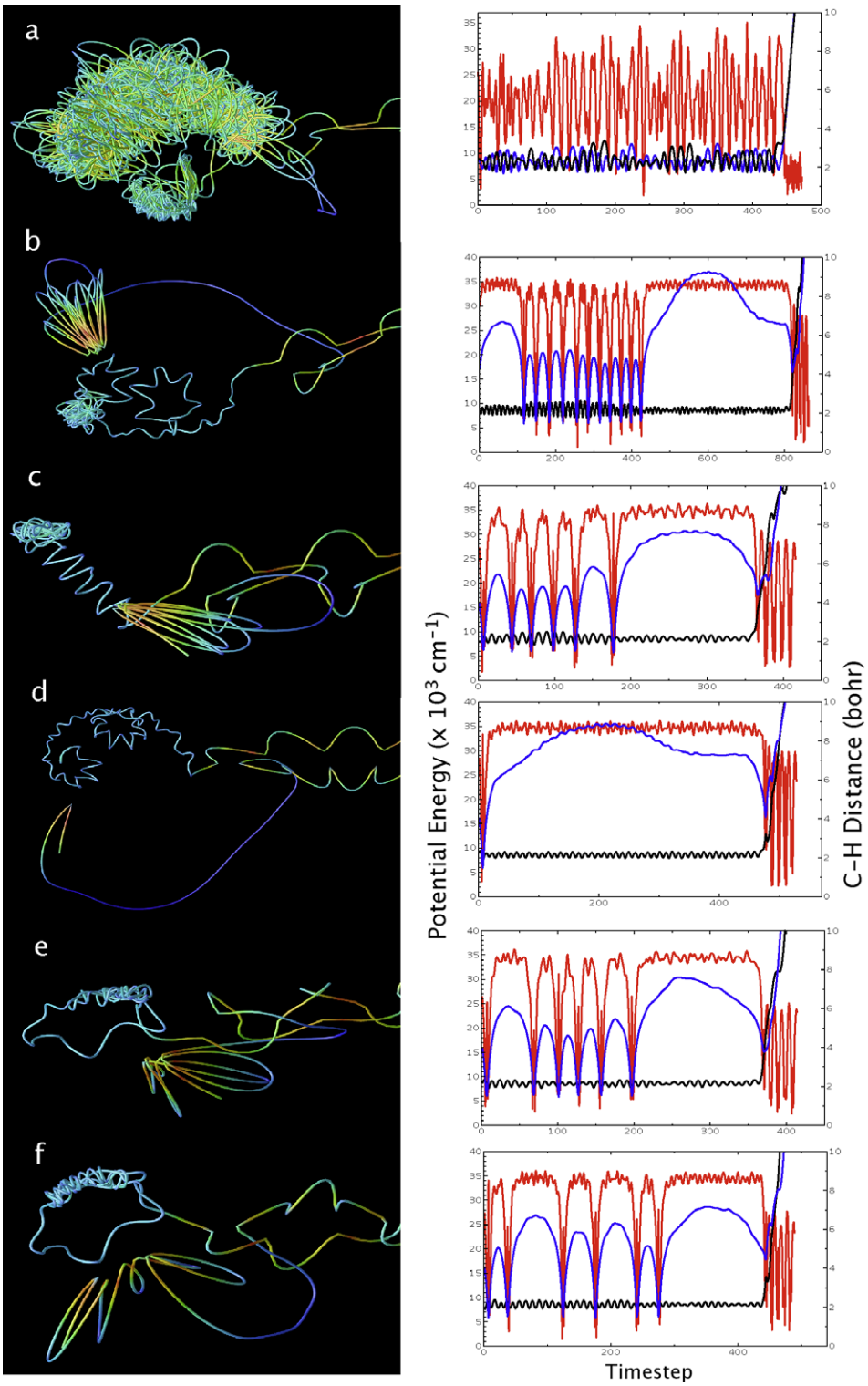

Fig. 8. H atom trajectory plots (left) and potential energy plots (right). The potential energy (red lines) are shown along with the C–H distances (roaming in blue, non-roaming, black). These trajectories yield the following CO and H_2 product states: (a) CO ($v = 0$, $j = 41$), H_2 ($v = 1$, $j = 7$) (nonroaming); (b) CO ($v = 0$, $j = 6$), H_2 ($v = 7$); (c) CO ($v = 0$, $j = 17$), H_2 ($v = 6$, $j = 7$); (d) CO ($v = 0$, $j = 9$), H_2 ($v = 6$, $j = 2$); (e) CO ($v = 0$, $j = 15$), H_2 ($v = 5$, $j = 10$); (f) CO ($v = 1$, j=22), H_2 ($v = 6$, $j = 5$). (For interpretation of the references to colour in this figure legend, the reader is referred to the web version of this article.)

$HCO–H_R$ orbital motion. The $C–H_R$ distance oscillates slightly but in the region of roaming and just prior to reaction it is roughly 7 bohr and in one example closer to 8 bohr. The former value is in good agreement, if slightly larger than, the 6.6 bohr value of the TS_R. We can also look closely at the total potential energy in the roaming

region to gain further insight. For the long roaming event in Fig. 8d, for example, the potential energy during the excursion reaches a minimum of 33,114 cm^{-1} and a maximum of 36,162 cm^{-1}. The difference between these values, ~3000 cm^{-1}, is essentially the vibrational excitation in the HCO, while the difference between the maximum and the available energy, ~328 cm^{-1}, must be in HCO rotation and HCO–H orbital motion.

Fig. 8 also demonstrates another key aspect of the roaming behavior: the roaming process and the abstraction are not coupled. This may be seen most clearly in Fig. 8f, in which two distinct roaming regions are seen, both exceeding 6.6 bohr C–H_R, and both showing high average potential energy values. The initial roaming excursion may be seen in the trajectory image as the first loop, where the trajectory also becomes deep blue showing very slow H atom motion. The C–H_R distance reaches 6.6 bohr and the potential energy averages 32,850 cm^{-1} in that region. It seems clear reaction will occur only if the roaming atom accesses the appropriate configuration during its explorations, and it is not simply a matter of C–H distance.

Here we have considered channel 3 in the vicinity of the radical threshold, where the near dissociation must correspond to formation of HCO in its lowest quantum states. However, we have seen that roaming also occurs above this threshold, and grows in importance relative to channel 1. This "roaming window" picture provides a basis for understanding the nature of the roaming motion at higher energies as well. We can separate the internal degrees of freedom of HCO from the roaming process and the low-frequency motions of TS_R. This is essentially a vibrationally adiabatic picture of the roaming dynamics. This is supported by the TS_R vibrational frequencies [45], 159i, 22, 83, 1114 1873 and 2739 cm^{-1}, the last three of which may be compared to HCO frequencies of 1114, 1874 and 2740 at the same level of theory. This close comparison clearly indicates that the saddle point represents essentially free HCO with a loosely bound H atom. If there is more energy in the radical dissociation coordinate than necessary to form H with HCO in a given quantum state, then roaming will not occur and radical dissociation will be the outcome. If the system possesses an energy in the range 0–100 cm^{-1} below this threshold, then roaming motion can occur leading to intramolecular abstraction. Finally, if the system is not within ~100 cm^{-1} of threshold for formation of HCO in a given quantum state, then roaming will not occur unless there is coupling of the HCO excitation into the low frequency modes. In this picture, the 100 cm^{-1} window may be considered to exist below each asymptotic HCO product state. This is schematically illustrated in Fig. 9a and b. In Fig. 9b, we show all possible product HCO energy levels, as well as those for the more likely $K_a = 1$ product states. In addition, we show a rectangle representing our nominal 100 cm^{-1} roaming "window", as well as the available transitions in S_1 for formaldehyde that we use to access these various energies (Fig. 9a). It is clear if we consider this 100 cm^{-1} roaming window, even just scanned across the sparse $K_a = 1$ states, the result is a continuum of energies at which roaming is readily possible. It is interesting to speculate whether the fluctuations in HCO product density of states seen in the diagram could give rise to fluctuations in the roaming yield. Our initial attempts to see evidence of this have not proved fruitful. One of the challenges, as may be seen in the diagram, is that there happen to be no states in S_1 we can use to access the sparsest regions of state density in HCO.

5.2. Roaming at high energy

At excitation energies higher than the threshold of the triplet surface dissociation, channel 4, it becomes dominant [12,34]. However, Fig. 4 provides clear evidence of dissociation via channel 3 above the threshold of channel 4. PHOFEX scans in this energy region (not shown here) revealed that 35217 cm^{-1} is the highest energy where the roaming mechanism is observed. This energy is very close to the HCO secondary dissociation threshold, where roaming could not be supported by a bound HCO species. Fig. 4 also shows that even at very high energies, the internal energy distribution of product H_2 is governed by previously reported abstraction dynamics [14]. Vibrational excitation in H_2 is observed up to $v = 10$.

5.3. Roaming leading to vibrationally excited CO

Moore and coworkers have shown previously that dissociation of formaldehyde via channel 1 leads to vibrationally excited CO ($v = 1$) with a yield of ~15% for dissociation via the $2^1 4^3$ transition [20]. In the van Zee paper that originally suggested an alternative pathway to molecular products [10], evidence was seen for this process leading to CO ($v = 1$). This was also seen recently in the QCT calculations from the Bowman group [38]. The data in Fig. 5 provides direct experimental confirmation of roaming leading to vibrationally excited CO ($v = 1$). Fig. 5a shows that after dissociation via the $2^4 4^1$ band, the internal state distribution of H_2 formed in coincidence with CO ($v = 1$, $j = 14$) peaks at around $v = 6$, $j = 9$; $v = 7$, $j = 7$; $v = 8$, $j = 7$ of H_2. This is consistent with the roaming model, where it was shown that the H-abstraction is responsible for the vibrational excitation of H_2 [14]. Fig. 5b shows that the internal energy distribution of H_2 formed in coincidence with CO ($v = 1$, $j = 14$) following dissociation via the $2^1 4^3$ band peaks around $v = 6$, $j = 9$; $v = 7$, $j = 3$; $v = 8$, $j = 1$ of H_2. This is also in agreement with the roaming model [14]. However, constraints on the available energy restrict the higher rotational excitation in H_2 for dissociation via the $2^1 4^3$ level. Fig. 8f shows a roaming trajectory that gives rise to vibrationally excited CO product. It is interesting to note that there is nothing particularly significant to distinguish this trajectory from the others aside from an initial unsuccessful roaming event discussed above. The average potential energy and the oscillations in the potential energy do not suggest any precursor in the dynamics. It is reason-

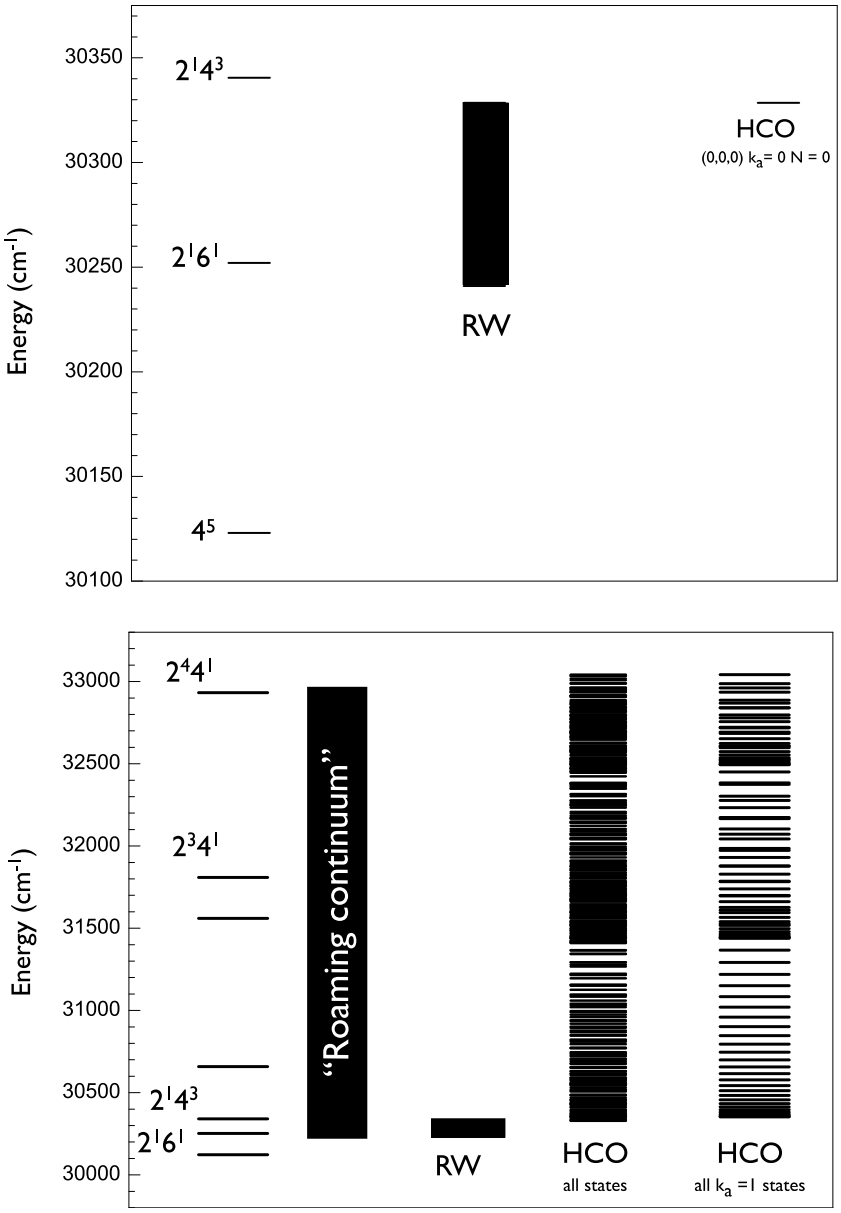

Fig. 9. Upper plot illustrates concept of the "roaming window" (RW) relative to the S1 levels near the radical threshold (see text). Lower plot shows numerous levels in S1 and possible HCO product states, along with "roaming continuum" formed by considering roaming to be possible 100 cm^{-1} below each HCO product state.

able that CO ($v = 1$) formation occurs directly in the abstraction step and depends on geometry and vibrational phases at that moment.

5.4. Nuclear spin conservation in roaming

Previous investigations of dissociation via channel 1 have shown conservation of nuclear spin during the dissociation [18]. The dissociation of *ortho*-formaldehyde via channel 1 results in the formation of *ortho*-H_2 and the dissociation of *para*-formaldehyde via channel 1 result in formation of *para*-H_2. Fig. 6 shows similarly that nuclear spin is largely conserved during the dissociation via channel 3, since *ortho*-formaldehyde clearly gives rise primarily to odd rotational levels implying *ortho*-H_2, while *para*-formaldehyde yields even rotational levels implying *para*-H_2. This is not surprising, as nuclear spin relaxation is very slow in general; in formaldehyde at room temperature it was measured by Moore et al. and found to be $\sim 0.1\ s^{-1}$ [18].

6. Conclusion

A comprehensive investigation of the roaming mechanism in formaldehyde dissociation is reported. Here all possible energy regions in the formaldehyde absorption spectrum leading to dissociation via channel 3 are covered. The threshold of channel 3 is between 30,240 and 30,123 cm^{-1}, largely consistent with a transition state

'region' suggested by Harding et al. The energy dependence of the roaming pathway is presented in terms of a "roaming window" that views the internal excitations of HCO as isolated from the roaming and abstraction event. The dissociation via channel 3 is not observed above 35,217.4 cm^{-1} owing to the opening of three-body dissociation processes that cannot support roaming. The dissociation via channel 3 also leads to vibrationally excited CO and its dynamics are governed by the previously reported roaming atom model. Nuclear spin is largely conserved during the dissociation of formaldehyde via channel 3.

Acknowledgements

A.G.S. thanks Dr. Greg Hall for many helpful discussions. This work was supported by the Director, Office of Science, Office of Basic Energy Sciences, Division of Chemical Sciences, Geosciences and Biosciences, of the US Department of Energy under contracts DE-FG02-04ER15593 (A.G.S.) and DE-FG02-97ER14782 (J.M.B.).

References

[1] G.H. Dieke, G.B. Kistiakowsky, Phys. Rev. 45 (1934) 4.
[2] G.H. Dieke, G.B. Kistiakowsky, Proc. Natl. Acad. Sci. 18 (1932) 367.
[3] B.A. DeGraff, J.G. Calvert, J. Am. Chem. Soc. 89 (1967) 2247.
[4] R.D. McQuigg, PhD, Ohio State University, Columbus, OH, 1965.
[5] J.A. Pople, J.W. Sidman, J. Chem. Phys. 27 (1957) 1270.
[6] R.G. Miller, E.K.C. Lee, Chem. Phys. Lett. 27 (1974) 475.
[7] P.L. Houston, C.B. Moore, J. Chem. Phys. 65 (1976) 757.
[8] C.B. Moore, J.C. Weisshaar, Annu. Rev. Phys. Chem. 34 (1983) 525.
[9] J. Troe, J. Phys. Chem. 88 (1984) 4375.
[10] R.D. van Zee, M.F. Foltz, C.B. Moore, J. Chem. Phys. 99 (1993) 1664.
[11] A.C. Terentis, S.H. Kable, Chem. Phys. Lett. 258 (1996) 626.
[12] L.R. Valachovic, M.F. Tuchler, M. Dulligan, T. Droz-Georget, M. Zyrianov, A. Kolessov, H. Reisler, C. Wittig, J. Chem. Phys. 112 (2000) 2752.
[13] D. Townsend, S.A. Lahankar, S.K. Lee, S.D. Chambreau, A.G. Suits, X. Zhang, J. Rheinecker, L.B. Harding, J.M. Bowman, Science 306 (2004) 1158.
[14] S.A. Lahankar, S.D. Chambreau, D. Townsend, F. Suits, J. Farnum, X. Zhang, J.M. Bowman, A.G. Suits, J. Chem. Phys. 125 (2006) 044303.
[15] S.A. Lahankar, S.D. Chambreau, X. Zhang, J.M. Bowman, A.G. Suits, J. Chem. Phys. 126 (2007), 044314/1-14/8.
[16] G.D. Smith, L.T. Molina, M.J. Molina, J. Phys. Chem. A 106 (2002) 1233.
[17] P. Ho, D.J. Bamford, R.J. Buss, Y.T. Lee, C.B. Moore, J. Chem. Phys. 76 (1982) 3630.
[18] B. Schramm, D.J. Bamford, C.B. Moore, Chem. Phys. Lett. 98 (1983) 305.
[19] D. Debarre, M. Lefebvre, M. Pealat, J.P.E. Taran, D.J. Bamford, C.B. Moore, J. Chem. Phys. 83 (1985) 4476.
[20] D.J. Bamford, S.V. Filseth, M.F. Foltz, J.W. Hepburn, C.B. Moore, J. Chem. Phys. 82 (1985) 3032.
[21] K.L. Carleton, T.J. Butenhoff, C.B. Moore, J. Chem. Phys. 93 (1990) 3907.
[22] T.J. Butenhoff, K.L. Carleton, C.B. Moore, J. Chem. Phys. 92 (1990) 377.
[23] T.J. Butenhoff, PhD, University of California, Berkeley, CA, 1990.
[24] T.J. Butenhoff, K.L. Carleton, R.D. Van Zee, C.B. Moore, J. Chem. Phys. 94 (1991) 1947.
[25] W.H. Green Jr., C.B. Moore, W.F. Polik, Annu. Rev. Phys. Chem. 43 (1992) 591.
[26] R.D. Van Zee, C.D. Pibel, T.J. Butenhoff, C.B. Moore, J. Chem. Phys. 97 (1992) 3235.
[27] S.D. Chambreau, S.A. Lahankar, A.G. Suits, J. Chem. Phys. 125 (2006) 044302.
[28] M. Dupuis, W.A. Lester Jr., B.H. Lengsfield III, B. Liu, J. Chem. Phys. 79 (1983) 6167.
[29] J.D. Goddard, H.F. Schaefer, J. Chem. Phys. 70 (1979) 5117.
[30] J.D. Goddard, Y. Yamaguchi, H.F. Schaefer III, J. Chem. Phys. 75 (1981) 3459.
[31] H.B. Schlegel, S.S. Iyengar, X. Li, J.M. Millam, G.A. Voth, G.E. Scuseria, M.J. Frisch, J. Chem. Phys. 117 (2002) 8694.
[32] M.J. Frisch, R. Krishnan, J.A. Pople, J. Phys. Chem. 85 (1981) 1467.
[33] H.M. Yin, K. Nauta, S.H. Kable, J. Chem. Phys. 122 (2005), 194312/1-12/10.
[34] H.M. Yin, S.H. Kable, X. Zhang, J.M. Bowman, Science 311 (2006) 1443.
[35] S.E. Waugh, A.C. Terentis, G.F. Metha, S.H. Kable, Proc. SPIE – Int. Soc. Opt. Eng. 3271 (1998) 36.
[36] A.C. Terentis, P.T. Knepp, S.H. Kable, Proc. SPIE – Int. Soc. Opt. Eng. 2548 (1995) 328.
[37] A.C. Terentis, S.E. Waugh, G.F. Metha, S.H. Kable, J. Chem. Phys. 108 (1998) 3187.
[38] X. Zhang, J.L. Rheinecker, J.M. Bowman, J. Chem. Phys. 122 (2005) 114313.
[39] L.B. Harding, S.J. Klippenstein, A.W. Jasper, Phys. Chem. Chem. Phys. 31 (2007) 4055.
[40] D. Townsend, M.P. Minitti, A.G. Suits, Rev. Sci. Instrum. 74 (2003) 2530.
[41] W. Li, S.D. Chambreau, S.A. Lahankar, A.G. Suits, Rev. Sci. Instrum. 76 (2005), 063106/1-06/7.
[42] A.V. Komissarov, M.P. Minitti, A.G. Suits, G.E. Hall, J. Chem. Phys. 124 (2006) 14303.
[43] X. Zhang, S. Zou, L.B. Harding, J.M. Bowman, J. Phys. Chem. A 108 (2004) 8980.
[44] D. Farnum John, X. Zhang, M. Bowman Joel, J. Chem. Phys. 126 (2007) 134305.
[45] L.B. Harding, Personal Communication.